

Interactions of PP-PET blends modified by montmorillonite with different polarities

Ariane Sarzi Porto¹ , Jefferson Lopes Alves²  and Ana Rita Morales^{1*} 

¹*Laboratório de Blendas e Compósitos Poliméricos, Departamento de Engenharia de Materiais e de Bioprocessos, Universidade Estadual de Campinas – UNICAMP, Campinas, SP, Brasil*

²*Departamento de Engenharia Química, Centro de Pesquisa em Alimentos, Universidade de São Paulo – USP, São Paulo, SP, Brasil*

*morales@unicamp.br

Abstract

This paper describes the effects of adding organic montmorillonite clays (MMT) with different polarities (one polar and one non-polar) in recycled poly (ethylene terephthalate) (PET) and polypropylene (PP) blends. Styrene-Ethylene/Butylene-Styrene-maleic anhydride-graft (SEBS-g-MA) was used as a compatibilizer. MMT polarity was chosen based on the expected specific interaction of each clay with PET and PP. Samples were evaluated by wide angle X-ray diffraction, scanning electronic microscopy, differential scanning calorimetry, Fourier transform infrared spectroscopy, dynamic mechanical analysis and mechanical tests. The clays caused no statistical change in the mechanical properties high-concentration PET blends, but increased Young's modulus and decreased the elongation at break, tensile strength and impact strength of high-concentration PP blends. The different interactions between PET and SEBS-g-MA and the level of MMT exfoliation in each polymer-rich phase explained the results.

Keywords: *nanocomposites, blends, montmorillonite, compatibility.*

How to cite: Porto, A. S., Alves, J. L., & Morales, A. R. (2022). Interactions of PP-PET blends modified by montmorillonite with different polarities. *Polímeros: Ciência e Tecnologia*, 32(3), e2022032. <https://doi.org/10.1590/0104-1428.20220014>

1. Introduction

Recycling waste from different thermoplastic polymers is a challenge due to the incompatibility between materials of different polar characteristics and the partial loss of mechanical properties. Polymer blending is a widely known process of combining the properties of each polymeric component of the blend. Nanocomposites developed by using organic modified clays, particularly montmorillonite, as a reinforcing filler can often exhibit remarkable improved properties when compared to neat polymer, conventional composites^[1-3], blends^[4-6] or even biopolymers.^[7-9] Polypropylene (PP), a low-cost thermoplastic, has many interesting properties, such as high chemical and solvent resistance, easy molding, high fatigue and bending fracture resistance, good impact strength above 15 °C, and good thermal stability^[10]. Polyethylene terephthalate (PET) has a high melting point (~265°C) and presents an excellent relation between mechanical and thermal properties and production cost^[11]. Its applications include textile fibers, packaging processed via injection molding process, films, and engineering. Environmental issues have drawn interest in recycling polymers from household waste, with PET being one of the most recycled plastics worldwide^[11].

As global production of resins and fibers has increased from 2 Mt in 1950 to 380 Mt in 2015, recycling is crucial. The total amount of resins and fibers manufactured from

1950 to 2015 is 7800 Mt, and half of this number—3900 Mt—was produced in just the last 13 years^[12].

The largest groups of plastics produced are PE (36%), PP (21%), and PVC (12%), followed by PET, PUR, and PS (<10% each). Polyester—which is mostly PET—accounts for 70% of all PP&A (polyester, polyamide, and acrylic fibers) production. Together, these seven groups account for 92% of all plastics ever made. Approximately 42% of all non-fiber plastics have been used for packaging, which is predominantly composed of PE, PP and PET^[12].

Given this high consumption of plastics, recycling PP and PET becomes imperative as plastic waste has a huge negative impact on the natural environment. Recycling helps to reduce the pollution caused by waste.

Since PET is a polar polymer and PP a non-polar one, PET-PP blends require the use of a compatibilizing agent to achieve a fine morphology. A block or graft copolymer can be used to decrease interfacial tension, whereas PP/PET blends with Styrene-Ethylene/Butylene-Styrene-maleic anhydride-graft (SEBS-g-MA) in different amounts have shown significant changes in the morphology of blends, such as improved phase dispersion and better mechanical properties, especially impact strength^[13].

Besides compatibilizers, clay minerals are widely used to obtain nanocomposites. Among these minerals, organic

montmorillonite (MMT) stands out due to its multilayer structure and high aspect ratio. The polarity relationship between polymers and MMT is fundamental in blends, as shown by studies on PP^[14-16], PET^[17-20], and PP-PET blends^[21-23] with commercial MMT. Adding Cloisite® 10A to PP-PET blends improved the mechanical properties and the system retained the two-phase morphology, but the PET domains were shown to be smaller and with good adhesion at the interface with PP. The use of clay alone was therefore insufficient to make the polymers compatible, and optimal results were observed when maleic anhydride-grafted polypropylene was added^[22]. Location of the polar nanoclay in the PET matrix led to a refined morphology and changed the rheological behavior of PET-PP blends, which was attributed to the formation of clay network-like structures^[23].

None of these studies considered a mixture of MMT (polar and non-polar), as the blends involve both polar and non-polar polymers. To understand the interactions between polar and non-polar systems, this paper presents the effects of including a mixture of two MMT with different polarities, Cloisite® 20A (non-polar) and Cloisite® 30B (polar), on the properties of PP-PET and SEBS-g-MA blends. The formulations chosen for the system studied considered the possible interactions between the polar and non-polar groups (Figure 1).

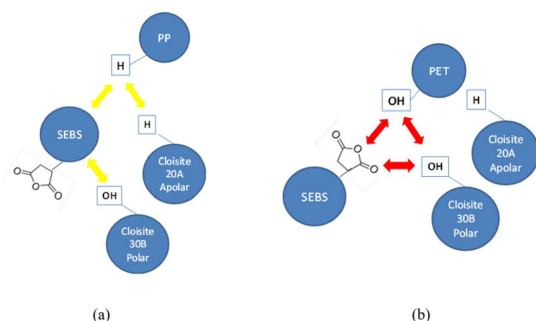


Figure 1. Interactions between (a) non-polar and (b) polar systems. Red arrows represent strong interactions, whereas yellow arrows represent weak interactions.

Table 1. Solubility parameter (Krevelen & Nijenhuis method^[24]).

Polymers and Clays	Solubility parameter (MJ/m ³) ^{1/2}
PET (Polar)	20.5
PP (Non-polar)	17.0
SEBS-g-MA (Polar)	21.0
Cloisite 30B (Polar)	19.0
Cloisite 20A (Non-polar)	15.9

Table 2. Sample compositions in % (w/w).

Sample	PP	PET	Cloisite 30B	Cloisite 20A	Irganox 1010	Compatibilizer SEBS-g-MA
PP30/PET70	29	68	-	-	1	2
PP70/PET30	68	29	-	-	1	2
PP70/PET30/MMT	65	28	2	2	1	2
PP30/PET70/MMT	28	65	2	2	1	2
PP	100	-	-	-	-	-
PET	-	100	-	-	-	-

2. Materials and Methods

2.1 Materials

We prepared the blends using PP pellets, MFI of 10 g/10min (RP 347, BRASKEM), recycled PET (GlobalPET), intrinsic viscosity of 0.72 dL/g, pellets size of 2.5 mm, MMT Cloisite® 20A and Cloisite® 30B (Southern Clays Products) modified with dimethyl di(hydrogenated tallow alkyl) and bis(2-hydroxyethyl) methyl (hydrogenated tallow alkyl) ammonium cations, respectively. SEBS-g-MA (FG-1901, KRATON), MFI of 22 g/10min functionalized with 2% maleic anhydride, was used as compatibilizer and 1% Irganox 1010 (BASF) as a thermal stabilizer.

2.2 Blend preparation

To evaluate the interaction aspects between polymers and MMT, we calculated the solubility parameters of the materials using the Krevelen & Nijenhuis method^[24] (Table 1). As can be observed, Cloisite 30B is expected to be more compatible with PET, whereas Cloisite 20A shows greater compatibility with PP. Hence, we chose a mixture of the organoclays to prepare the samples to study the presence of each clay in each blend phase.

Blends were prepared using melt intercalation. Table 2 presents the sample compositions.

Materials were dried in a circulating air oven at 100 °C for 60 min, extruded on a Haake Reomex OS PTW24 twin-screw at temperatures ranging from 240 to 275 °C, screw rotation of 250 rpm, torque of 46 N/m, and feed rate of 60%. The extruded pellets were dried in a circulating air oven at 100 °C for 60 min before being injected in a Boy 35 injection molding machine, at the temperatures of 260 °C (barrel), 270 °C (nozzle), and 60 °C (mold), according to ASTM D638-02 and ASTM D256-10 for tensile and impact tests, respectively.

Scanning electron microscopy (SEM) experiments were performed on the FEI Inspect 5S operating at 20 kV. The observed surfaces were obtained by cryogenic fracturing of the samples and coated with a gold layer. Wide angle X-ray diffraction (WAXD) experiments were performed on a Rigaku diffractometer, and the samples were scanned using CuK_α radiation (k = 1.5406 Å). The clay space gallery (d₀₀₁) was determined using Bragg's law for clays and nanocomposites. Tensile testing was conducted using the INSTRON 5582 testing machine according to ASTM D638-02, performed at 50 mm min⁻¹ speed under ambient conditions. Izod impact tests were performed by an EMIC impact machine according to ASTM D256-10e1 using an impact pendulum of 2.82 J. Values from the tensile tests Young's modulus (E), elongation at break (ε), tensile

strength at break (σ) and impact strength (IS), performed to evaluate the equality of blends with and without MMT, were submitted to analysis of variance (ANOVA). In statistical analysis, p-value is the significance probability used in hypothesis testing, defining: the null hypothesis (H_0), where means are equal; and the alternative hypothesis (H_A), where means are different. By confronting the null hypothesis with the average results from the studied sample, we verify its occurrence in probabilistic terms, which leads us to reject H_0 or not. If H_0 is not rejected, it is assumed to be true; otherwise, H_A is true. In this study, significance level was set at $\alpha = 0.05$, so when the p-value was less than or equal to α , H_0 was rejected and the means were considered different; for p-values greater than α , H_0 was accepted and the means were considered equal^[25]. Differential scanning calorimetry (DSC) curves were obtained by TA Instruments, model DSC Q100, with temperature ranging from $-90\text{ }^\circ\text{C}$ to $300\text{ }^\circ\text{C}$, under dynamic atmosphere of N_2 (50 mL min^{-1}) and a $10\text{ }^\circ\text{C min}^{-1}$ heating rate. Fourier transform infrared spectroscopy (FTIR) analysis was performed on a Thermo Nicolet iS50, scanning 4000 to 650 cm^{-1} in attenuated total reflection (ATR) mode. Dynamic mechanical analysis (DMA) was performed by a TA Instruments Q800 on $63.5 \times 12.7 \times 3.2\text{ mm}$ rectangular samples, at 3-Point Bend deformation mode, with a deformation amplitude of $60\text{ }\mu\text{m}$ determined using strain sweep tests to ensure a linear viscoelastic response of the material, temperature range of $-30\text{ }^\circ\text{C}$ to $230\text{ }^\circ\text{C}$, with $3\text{ }^\circ\text{C min}^{-1}$ heating rate and 1 Hz frequency.

3. Results and Discussions

Table 3 presents the mechanical results and Table 4 summarizes the ANOVA tests comparing the equality of the mean results between two populations: blends with and without MMT.

The presence of MMT in the PP30/PET70 and PP30/PET70MMT samples showed no statistical change between the populations regarding all measured mechanical properties,

indicating that MMT had no influence on these characteristics. In turn, the PP70/PET30 and PP70/PET30/MMT samples showed the opposite effect: the presence of MMT increased E (from 1342 MPa to 1504 MPa) and decreased ε (from 12% to 9%) and σ (from 26 MPa to 27 MPa). We also found that IS decreased from 6 J/m to 4 J/m .

Figure 2a shows the diffractograms for all samples and Figure 2b for the blends with and without clay. X-Ray diffractograms for the same Cloisite® 20A and Cloisite® 30B samples used in this study were published elsewhere and the authors described them as having basal space (d_{001}) of 2.69 nm ($2\theta = 3.28^\circ$) and 1.86 nm ($2\theta = 4.74^\circ$), respectively^[26]. In the X-Ray diffractograms of the blends in the region where the clay planes are detected, 2θ between 2 and 7° (Figure 2b), we observe a peak at 2.44° for sample PP30/PET70/MMT

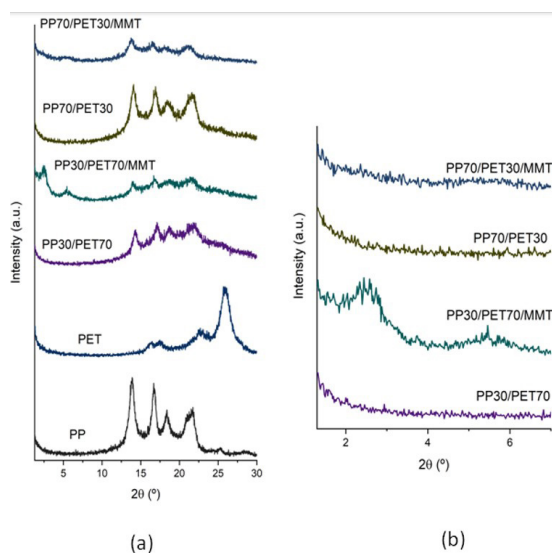


Figure 2. X-Ray diffractograms: (a) All samples and (b) PP30/PET70, PP30/PET70/MMT, PP70/PET30 and PP70/PET30/MMT.

Table 3. Modulus (E), Tensile stress at break (σ), Elongation (ε) and Impact resistance (IS).

Sample	σ max (MPa)	σ at break (MPa)	ε (%)	E (MPa)	IS (J/m)
Neat PP	34 ± 2	22 ± 5	194 ± 100	1359 ± 192	12 ± 2
Neat PET	55 ± 5	16 ± 10	123 ± 120	2315 ± 177	16.0 ± 0.2
PP30/PET70	38 ± 5	38 ± 4	4 ± 2	1920 ± 170	6.0 ± 0.9
PP30/PET70/MMT	41.0 ± 0.5	37 ± 2	5 ± 1	2009 ± 41	6.0 ± 0.8
PP70/PET30	29.7 ± 0.4	26 ± 2	12 ± 2	1342 ± 106	6.0 ± 1.0
PP70/PET30/MMT	27.8 ± 0.4	27 ± 1	9 ± 2	1504 ± 65	4.0 ± 0.4

Table 4. ANOVA of Modulus (E), Tensile stress at break (σ), Elongation (ε) and Impact resistance (IS) ($\alpha = 0.05$).

Compared samples	Response	p-value	Statistical mean results	MMT influence	
PP30/PET70 and PP30/PET70/MMT	E (MPa)	0.289	Equal	No	
	σ (MPa)	0.211			
	ε (%)	0.123			
	IS (J/m)	0.622			
PP70/PET30 and PP70/PET30/MMT	E (MPa)	0.019	Different	Yes (from 1342 to 1504 MPa)	
	σ (MPa)	0.007			Yes (from 26 to 27 MPa)
	ε (%)	0.019			Yes (from 12 to 9%)
	IS (J/m)	0.029			Yes (from 6 to 4 J/m)

with $d_{001} = 3.62$ nm attributed to a first order peak of Cloisite® 20A non-polar clay. The second peak observed at 5.8° may be a second order peak of Cloisite® 20A^[22,26]. This Cloisite® 20A peak in the blend is shifted when compared to the neat clay signal, indicating that some of the Cloisite® 20A may have exfoliated and some may have intercalated. Absence of the Cloisite® 30B clay signal suggests that most of the clay exfoliated in the system. For the PP70/PET30/MMT samples, the absence of both neat clay peaks indicates that exfoliation may have occurred primarily for both the non-polar Cloisite® 20A and polar Cloisite® 30B.

SEM analysis indicated the two-phase morphology as expected, due to the non-miscibility between polymers (Figure 3). Adding MMT preserves the heterogeneous two-phase system, but the PP70/PET30/MMT sample shows changes in the morphology where the domains present a poorly defined interface. The system morphology was certainly modified, most likely due to clay exfoliation which probably decreased the interfacial tension and/or the coalescence restriction of the dispersed phase domains.

Figure 4 shows the DSC curves for the specimens subjected to mechanical tests. From the DSC results, we calculated the degree of crystallinity (W_c) using Equation 1 (Table 5):

$$w_c = \frac{(\Delta H_m - \Delta H_{cc})}{\Delta H_{m,100\%}} \times 100 \quad (1)$$

where ΔH_m is the measured melting enthalpy for each peak and $\Delta H_{m,100\%}$ the hypothetical equilibrium enthalpy considering the polymer to be 100% crystalline, assuming 140 J/g for PET and 207 J/g for isotactic PP homopolymer^[27]; ΔH_{cc} is the enthalpy of crystallization that occurs during heating, if applicable, called cold crystallization; and f is the mass fraction of the polymer present in the mixture.

Table 5. Degree of crystallinity – DSC and X-Ray deconvolution (WAXD).

Samples	DSC		WAXD
	PP	PET	Blends
PET	-	43	37
PP	43	-	49
PP70/PET30	26	27	19
PP70/PET30/ MMT	28	20	27
PP30/PET70	7	21	13
PP30/PET70/ MMT	4	22	20

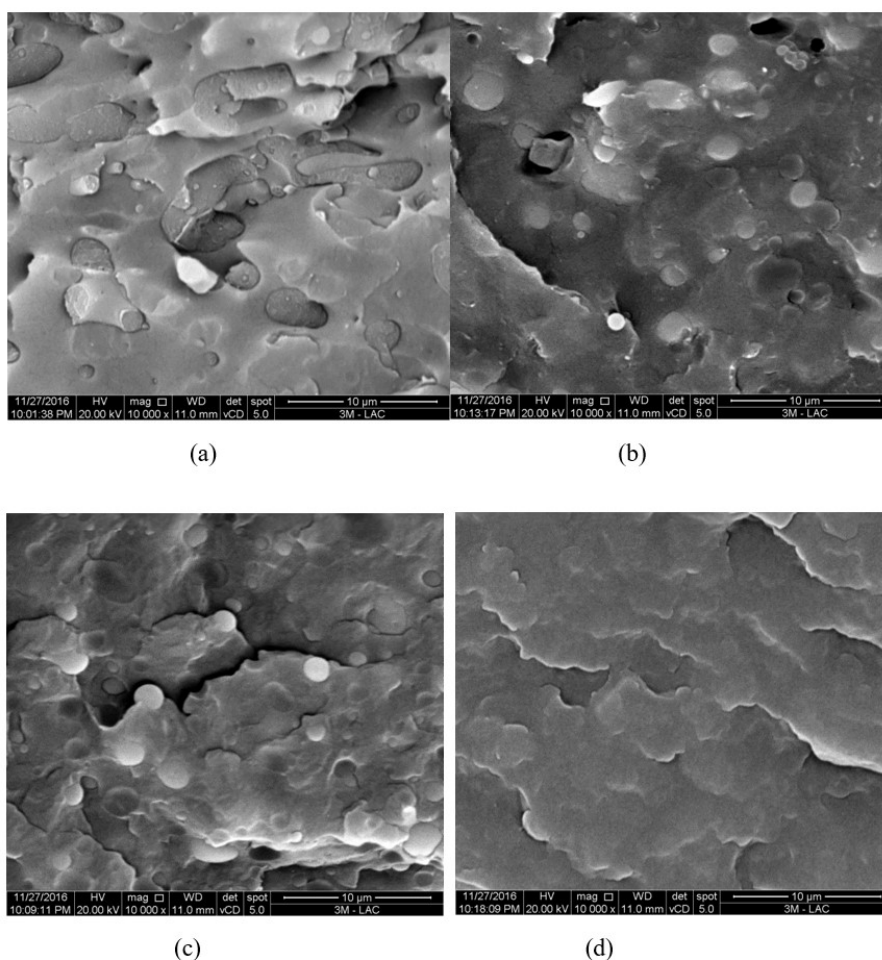


Figure 3. Photomicrographs from SEM analysis: (a) PP30/PET70, (b) PP30/PET70/MMT, (c) PP70/PET30 and (d) PP70/PET30/MMT.

The samples with higher PET content showed cold crystallization during the heating scan. Cold crystallization is related to the partial amorphous state of the polymer due to its slow crystallization rate: when a molten polymer is rapidly cooled, many crystalline nuclei are formed, but crystal growth is negligible. During the subsequent heating scan, amorphous regions rearrange into a crystalline phase and the crystalline nuclei grow, causing a rapid re-crystallization process that occurs between the glass transition temperature and the melting point of the polymer^[23]. This cold crystallization process overlaps with the PP melting signal; but since where the PP melting curve starts and ends is poorly defined, this can interfere with the calculation of the degree of crystallinity via DSC. Consequently, X-Ray could also help in determining the degree of crystallinity of the system. We thus calculated the degree of crystallinity of the blends using the Deconvolution Method and adjusting the peaks of the X-Ray diffraction pattern (Figure 2a). This method brings some considerations during adjustment, such as the shape and number of peaks observed in the diffractogram. Deconvolution is performed by computational programs that use functions—such as Gaussian ones—to adjust the curves from the crystalline contributions of each peak and the amorphous halo contribution. In this study, we used the ‘Fit Gaussian’ method, and the area of each peak led to a degree of crystallinity using Equation 2^[28]:

$$C = \frac{\sum A_{crystalline}}{\sum A_{crystalline} + \sum A_{amorphous}} 100(\%) \quad (2)$$

where $A_{crystalline}$ is the crystalline contribution of each peak and $A_{amorphous}$ the amorphous halo contribution. Table 5 summarizes the results obtained.

Given the DSC inconclusive results, including those from WAXD, the presence of MMT appears to increase the degree of crystallinity of the entire system in both pairs of samples: when comparing PP30/PET70 with PP30/PET70/MMT and PP70/PET30 with PP70/PET30/MMT. These results can explain the reduction in impact strength observed. High-density polyethylene nanocomposites with nanoclay showed a reduction in impact strength associated with an increase in the degree of polymer crystallinity near the clay/polymer interface^[29]. This local increase in the degree of crystallinity could lead to a more brittle system with less capacity to absorb impact energy. Given the observed increase in the degree of crystallinity of the system resulting from

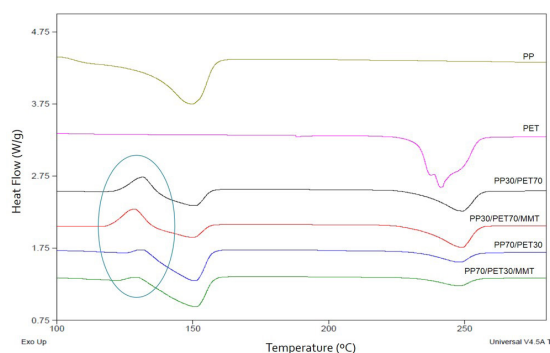


Figure 4. DSC curves showing cold crystallization of PET.

the clay, we can assume that, for the PP70/PET30/MMT sample, where the clay was highly exfoliated, PP may have crystallized more easily at the clay interface.

Table 6 describes the glass transition temperature determined from the DMA curves (not shown). We can observe that the Tg of the blends shows no significant change when compared to neat polymers, which points to the lack of miscibility between the polymers.

The FTIR spectrum (Figure 5) shows typical absorption bands for the CH bonds present in PP, the stretching of CH/CH₂/CH₃ groups ranged from 2850 to 2980 cm⁻¹, the angular deformation of CH₃ groups varied between 1354 and 1460 cm⁻¹, the stretching of C-C bonds at 1167 cm⁻¹ and the angular deformation of C-H groups at 890 cm⁻¹. PET shows important bands at 1710 cm⁻¹ due the stretching of ester carbonyl groups, and at 1410 cm⁻¹ due to the stretching of C = C bonds in the aromatic ring.

SEBS-g-MA, the compatibilizer used in this study, contains maleic anhydride that could react with polar PET groups. Although the amount of SEBS-g-MA was small and at 2% MA, the change in the absorption band at 1710 cm⁻¹ due to the carbonyl of carboxylic groups suggests that the reaction may have occurred^[30,31]. To normalize the FTIR peaks and verify the extent of this reaction, we chose the band of neutral aromatic group at 1410 cm⁻¹ since the aromatic ring of PET is unchanged.

Despite the degree of uncertainty in the deconvolution method due to the integration of the absorption bands, it appears to be a good estimate for the ratio between the area of the 1710 cm⁻¹ (A_{1710}) and 1410 cm⁻¹ (A_{1410}) absorption bands (Table 7). The relation between these peaks indicates

Table 6. Glass transition temperatures determined from DMA curves.

Sample	Tg PP (°C)	Tg PET (°C)
PP	-1 ± 1	-
PET	-	80 ^[22]
PP30/PET70	-8 ± 3	84 ± 6
PP30/PET70/MMT	-5 ± 1	78 ± 4
PP70/PET30	-2 ± 1	78 ± 1
PP70/PET30/MMT	-1 ± 1	83 ± 7

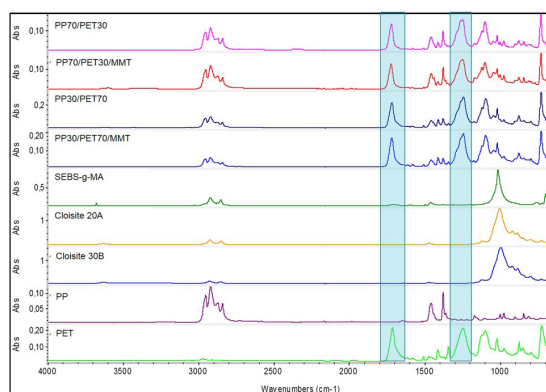


Figure 5. FTIR spectrum of the samples, indicating bands at 1710 and 1410 cm⁻¹.

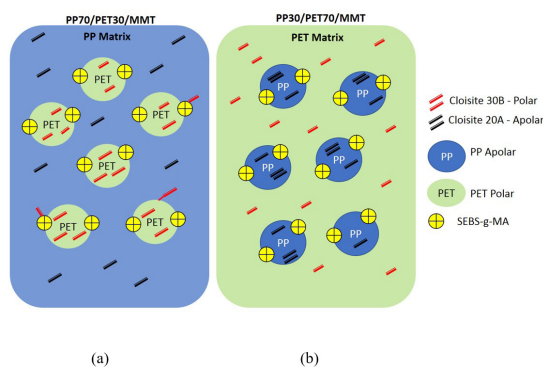
Table 7. Ratio between the area of the 1710 cm^{-1} and 1410 cm^{-1} bands.

Sample	A_{1710} / A_{1410}
PET	8
PP30/PET70	12
PP30/PET70/MMT	13
PP70/PET30	15
PP70/PET30/MMT	24

that both PP30/PET70 and PP70/PET30 blends saw an increase in the number of free carboxyl groups, that is, maleic anhydride probably reacted in these cases, opening its ring and covalently binding the PET polymer, increasing the ester groups in the system and thus causing some compatibilization between PP and PET at the interface.

After adding clay to the PP30/PET70/MMT system, the ratio remained about the same when compared to sample PP30/PET70. In the system with more PP (PP70/PET30/MMT), the ratio increased from 15 to 24. This result shows that besides the reaction between PET and SEBS-g-MA, the OH groups of the polar clay are highly likely to react with SEBS-g-MA in this system, increasing their compatibilization.

Figure 6 depicts the suggested scheme that may explain the behavior of the studied system. SEBS-g-MA tends to remain at the interface and interact with both polymers, but chemically reacts with PET (as the comparative FTIR analysis shows an increase in ester groups, which occurred due to the reaction between MA groups and the PET chain terminals). For sample PP70/PET30/MMT, the X-Ray diffraction analysis shows that the peaks of the neat clays seem to disappear. Thus, we hypothesize that both the polar Cloisite® 30B clay and the non-polar Cloisite® 20A clay have exfoliated in our sample. This behavior is evidenced in the SEM analysis, by comparing Figures 3c and 3d, where the PP70/PET30/MMT system showed reduction in the domains and a poorly defined interface, probably due to clay exfoliation. Cloisite® 20A is exfoliated in the PP domains, whereas Cloisite®30B is exfoliated in the PET matrix. PET is predominantly in the dispersed phase. In the PP30/PET70/MMT sample, PET is predominantly in the continuous phase where Cloisite®30B is exfoliated. The dispersed phase is a PP-rich phase where the non-polar Cloisite® 20A clay is still present, indicating that some of it may have been intercalated and some exfoliated, as observed by X-Ray analysis. In the literature, Cloisite® 20A incorporated into PP blends with other polymers was described to be predominantly localized in the continuous phase and at the interface causing a reduction in the size of the dispersed polymer phase domains and was attributed to act as a barrier and decrease interfacial tension between the components, acting as a compatibilizer^[32]. Similarly, the PP/PA blends where Cloisite® 30B was used due to its affinity to PA, showed to be mainly located at the interface which inhibited coalescence and caused the reduction of PA domains^[33]. Improved interface and reduced well-defined domains (observed in the SEM images) can be attributed to the good chemical interface between PET and SEBS-g-MA caused by the chemical ring-opening reaction of the maleic anhydride. Despite this significant improvement

**Figure 6.** Schematic morphology and component distribution: (a) PP70/PET30/MMT and (b) PP30/PET70/MMT.

in the interface, we observed no significant change in the mechanical properties of the system.

4. Conclusions

Organic montmorillonite clays with different polarities have shown to improve the compatibility of the system studied. The PP-rich blend was statistically modified by the addition of different MMT polarity, although the higher affinity of the polar MMT with PET and the non-polar MMT with PP. This can be attributed to the exfoliated clays, which led to a reduction in the domains as observed by SEM. Adding SEBS-g-MA resulted in a good adhesion between the phases, probably because SEBS-g-MA reacted with PET, increasing the compatibility of the system. Besides this reaction, the OH group of polar Cloisite® 30B may have had a strong interaction with both the compatibilizer and PET. The increased degree of blend crystallinity could be explained by the organization of lamellae at the clay/polymer interface, which leads to a more brittle system with less capacity to absorb impact energy. This study hypothesizes about how and where different organically modified clays are dispersed to the incompatible polymer system and contributes to a better understanding on the interactions that may occur, opening new possibilities for future studies on thermoplastic polymer reuse.

5. Author's Contribution

- **Conceptualization** – Ana Rita Morales.
- **Data curation** – Ariane Sarzi Porto.
- **Formal analysis** – Ariane Sarzi Porto; Jefferson Lopes Alves.
- **Funding acquisition** – Ana Rita Morales.
- **Investigation** – Ariane Sarzi Porto.
- **Methodology** – Ariane Sarzi Porto; Ana Rita Morales; Jefferson Lopes Alves.

- **Project administration** – Ariane Sarzi Porto; Ana Rita Morales.
- **Resources** – Ariane Sarzi Porto; Ana Rita Morales.
- **Software** – NA.
- **Supervision** – Ana Rita Morales.
- **Validation** – NA.
- **Visualization** – Ariane Sarzi Porto; Ana Rita Morales; Jefferson Lopes Alves.
- **Writing – original draft** – Ariane Sarzi Porto.
- **Writing – review & editing** – Ana Rita Morales; Jefferson Lopes Laves.

6. Acknowledgements

The authors thank GlobalPet and Southern Clay Products for supplying the sample materials; 3M, IPEN/USP, UFRJ and Thermoblend for supporting the analysis; Espaço da Escrita – Pró-Reitoria de Pesquisa – UNICAMP – for the language services provided; and FAEPEX/UNICAMP for the article publication charge.

7. References

1. Manias, E., Touny, A., Wu, L., Strawhecker, K., Lu, B., & Chung, T. C. (2001). Polypropylene/montmorillonite nanocomposites. Review of the synthetic routes and materials properties. *Chemistry of Materials*, *13*(10), 3516-3523. <http://dx.doi.org/10.1021/cm0110627>.
2. Weng, Z., Wang, J., Senthil, T., & Wu, L. (2016). Mechanical and thermal properties of ABS/montmorillonite nanocomposites for fused deposition modeling 3D printing. *Materials & Design*, *102*, 276-283. <http://dx.doi.org/10.1016/j.matdes.2016.04.045>.
3. Wang, Y., Wu, G., Kou, K., Pan, C., & Feng, A. (2016). Mechanical, thermal conductive and dielectrical properties of organic montmorillonite reinforced benzoxazine/cyanate ester copolymer for electronic packaging. *Journal of Materials Science Materials in Electronics*, *27*(8), 8279-8287. <http://dx.doi.org/10.1007/s10854-016-4834-5>.
4. Zhou, J., Yao, Z., Zhou, C., Wei, D., & Li, S. (2014). Mechanical properties of PLA/PBS foamed composites reinforced by organophilic montmorillonite. *Journal of Applied Polymer Science*, *131*(18), 40773. <http://dx.doi.org/10.1002/app.40773>.
5. Magalhães, N. F., Dahmouche, K., Lopes, G. K., & Andrade, C. T. (2013). Using an organically-modified montmorillonite to compatibilize a biodegradable blend. *Applied Clay Science*, *72*, 1-8. <http://dx.doi.org/10.1016/j.clay.2012.12.008>.
6. Sengwa, R. J., Choudhary, S., & Sankhla, S. (2010). Dielectric properties of montmorillonite clay filled poly(vinyl alcohol)/poly(ethylene oxide) blend nanocomposites. *Composites Science and Technology*, *70*(11), 1621-1627. <http://dx.doi.org/10.1016/j.compscitech.2010.06.003>.
7. Cyrus, V. P., Manfredi, L. B., Ton-That, M.-T., & Vázquez, A. (2008). Physical and mechanical properties of thermoplastic starch/montmorillonite nanocomposite films. *Carbohydrate Polymers*, *73*(1), 55-63. <http://dx.doi.org/10.1016/j.carbpol.2007.11.014>.
8. Chen, X., Gao, H., & Ploehn, H. J. (2014). Montmorillonite-levan nanocomposites with improved thermal and mechanical properties. *Carbohydrate Polymers*, *101*, 565-573. <http://dx.doi.org/10.1016/j.carbpol.2013.09.073>. PMID:24299812.
9. Jollands, M., & Gupta, R. K. (2010). Effect of mixing conditions on mechanical properties of polylactide/montmorillonite clay nanocomposites. *Journal of Applied Polymer Science*, *118*(3), 1489-1493. <http://dx.doi.org/10.1002/app.32475>.
10. Maddah, H. A. (2016). Polypropylene as a promising plastic: a review. *American Journal of Political Science*, *6*(1), 1-11. <http://dx.doi.org/10.5923/j.ajps.20160601.01>.
11. Romão, W., Spinacé, M. A. S., & De Paoli, M.-A. (2009). Poly(ethylene terephthalate), PET: a review on the synthesis processes, degradation mechanisms and its recycling. *Polímeros: Ciência e Tecnologia*, *19*(2), 121-132. <http://dx.doi.org/10.1590/S0104-14282009000200009>.
12. Geyer, R., Jambeck, J. R., & Law, K. L. (2017). Production, use, and fate of all plastics ever made. *Science Advances*, *3*(7), e1700782. <http://dx.doi.org/10.1126/sciadv.1700782>. PMID:28776036.
13. Araujo, L. M. G., & Morales, A. R. (2018). Compatibilization of recycled polypropylene and recycled poly (ethylene terephthalate) blends with SEBS-g-MA. *Polímeros: Ciência e Tecnologia*, *28*(1), 84-91. <http://dx.doi.org/10.1590/0104-1428.03016>.
14. Paiva, L. B., Morales, A. R., & Guimarães, T. R. (2006). Propriedades mecânicas de nanocompósitos de polipropileno e montmorilonita organofílica. *Polímeros: Ciência e Tecnologia*, *16*(2), 136-140. <http://dx.doi.org/10.1590/S0104-14282006000200014>.
15. Komatsu, L. G. H., Oliani, W. L., Lugao, A. B., & Parra, D. F. (2014). Environmental ageing of irradiated polypropylene/montmorillonite nanocomposites obtained in molten state. *Radiation Physics and Chemistry*, *97*, 233-238. <http://dx.doi.org/10.1016/j.radphyschem.2013.12.004>.
16. Kim, D. H., Fasulo, P. D., Rodgers, W. R., & Paul, D. R. (2007). Structure and properties of polypropylene-based nanocomposites: effect of PP-g-MA to organoclay ratio. *Polymer*, *48*(18), 5308-5323. <http://dx.doi.org/10.1016/j.polymer.2007.07.011>.
17. Kráčalík, M., Mikešová, J., Puffr, R., Baldrian, J., Thomann, R., & Friedrich, C. (2007). Effect of 3D structures on recycled PET/organoclay nanocomposites. *Polymer Bulletin*, *58*(1), 313-319. <http://dx.doi.org/10.1007/s00289-006-0592-5>.
18. Kráčalík, M., Studenovský, M., Mikešová, J., Sikora, A., Thomann, R., Friedrich, C., Fortelný, I., & Šimoník, J. (2007). Recycled PET nanocomposites improved by silanization of organoclays. *Journal of Applied Polymer Science*, *106*(2), 926-937. <http://dx.doi.org/10.1002/app.26690>.
19. Kráčalík, M., Studenovský, M., Mikešová, J., Kovářová, J., Sikora, A., Thomann, R., & Friedrich, C. (2007). Recycled PET-organoclay nanocomposites with enhanced processing properties and thermal stability. *Journal of Applied Polymer Science*, *106*(3), 2092-2100. <http://dx.doi.org/10.1002/app.26858>.
20. Gurmendi, U., Eguiazabal, J. I., & Nazabal, J. (2007). Structure and properties of nanocomposites with a poly(ethylene terephthalate) matrix. *Macromolecular Materials and Engineering*, *292*(2), 169-175. <http://dx.doi.org/10.1002/mame.200600376>.
21. Calcagno, C. I. W., Mariani, C. M., Teixeira, S. R., & Mauler, R. S. (2009). Morphology and crystallization behavior of the PP/PET nanocomposites. *Journal of Applied Polymer Science*, *111*(1), 29-36. <http://dx.doi.org/10.1002/app.28977>.
22. Calcagno, C. I. W., Mariani, C. M., Teixeira, S. R., & Mauler, R. S. (2008). The role of the MMT on the morphology and mechanical properties of the PP/PET blends. *Composites Science and Technology*, *68*(10-11), 2193-2200. <http://dx.doi.org/10.1016/j.compscitech.2008.03.012>.

23. Entezam, M., Khonakdar, H. A., Yousefi, A. A., Jafari, S. H., Wagenknecht, U., & Heinrich, G. (2013). Dynamic and transient shear start-up flow experiments for analyzing nanoclay localization in PP/PET blends: correlation with microstructure. *Macromolecular Materials and Engineering*, 298(1), 113-126. <http://dx.doi.org/10.1002/mame.201100435>.
24. Van Krevelen, D. W., & Nijenhuis, K. T. (2009). *Properties of polymers. Their correlation with chemical structure: their numerical estimation and prediction from additive group contributions*. Netherlands: Elsevier.
25. Kim, T. K. (2017). Understanding one-way ANOVA using conceptual figures. *Korean Journal of Anesthesiology*, 70(1), 22-26. <http://dx.doi.org/10.4097/kjae.2017.70.1.22>. PMID:28184262.
26. Souza, P. M. S., Morales, A. R., Marin-Morales, M. A., & Mei, L. H. I. (2014). Estudo da influência de argilas organofílicas no processo de biodegradação do PLA. *Polímeros Ciência e Tecnologia*, 24(1), 110-116. <http://dx.doi.org/10.4322/polimeros.2014.058>.
27. Wunderlich, B. (1990). *Thermal analysis*. USA: Academic Press, Inc. <http://dx.doi.org/10.1016/B978-0-12-765605-2.50006-6>.
28. Nagaraj, S. K., Shivanna, S., Subramani, N. K., & Siddaramaiah, H. (2016). Revisiting powder x-ray diffraction technique: a powerful tool to characterize polymers and their composite films. *Research, & Reviews. Journal of Materials Science*, 4(4), 1-5. <http://dx.doi.org/10.4172/2321-6212.1000158>.
29. Tanniru, M., Yuan, Q., & Misra, R. D. K. (2006). On significant retention of impact strength in clay-reinforced high-density polyethylene (HDPE) nanocomposites. *Polymer*, 47(6), 2133-2146. <http://dx.doi.org/10.1016/j.polymer.2006.01.063>.
30. Liu, N. C., & Baker, W. E. (1992). Reactive polymers for blend compatibilization. *Advances in Polymer Technology*, 11(4), 249-262. <http://dx.doi.org/10.1002/adv.1992.060110403>.
31. Orr, C. A., Cernohous, J. J., Guegan, P., Hirao, A., Jeon, H. K., & Macosko, C. W. (2001). Homogeneous reactive coupling of terminally functional polymers. *Polymer*, 42(19), 8171-8178. [http://dx.doi.org/10.1016/S0032-3861\(01\)00329-9](http://dx.doi.org/10.1016/S0032-3861(01)00329-9).
32. Chandran, N., Chandran, S., Maria, H. J., & Thomas, S. (2015). Compatibilizing action and localization of clay in a polypropylene/natural rubber (PP/NR) blend. *RSC Advances*, 5(105), 86265-86273. <http://dx.doi.org/10.1039/C5RA14352G>.
33. Beuguel, Q., Ville, J., Crepin-Leblond, J., Mederic, P., & Aubry, T. (2017). Influence of clay mineral structure and polyamide polarity on the structural and morphological properties of clay polypropylene/polyamide nanocomposites. *Applied Clay Science*, 135, 253-259. <http://dx.doi.org/10.1016/j.clay.2016.09.034>.

Received: Mar. 03, 2022

Revised: Jun. 20, 2022

Accepted: Aug. 04, 2022